Dual Photo- and pH-Responsive Supramolecular Nanocarriers Based on Water-Soluble Pillar[6]arene and Different Azobenzene Derivatives for Intracellular Anticancer Drug Delivery

ARTICLE *in* CHEMISTRY - A EUROPEAN JOURNAL · NOVEMBER 2014

Impact Factor: 5.73 · DOI: 10.1002/chem.201405095

9 AUTHORS, INCLUDING:

Xiao-Yu Hu
Nanjing University
35 PUBLICATIONS **863** CITATIONS
SEE PROFILE

Yan Li
Anhui
7 PUBLICATIONS **218** CITATIONS
SEE PROFILE

Fan Zhou
Nanjing University
1 PUBLICATION **10** CITATIONS
SEE PROFILE

ChemPubSoc Europe

DOI: 10.1002/chem.201405095

CHEMISTRY
A European Journal
Full Paper

Drug Delivery

Dual Photo- and pH-Responsive Supramolecular Nanocarriers Based on Water-Soluble Pillar[6]arene and Different Azobenzene Derivatives for Intracellular Anticancer Drug Delivery

Xiao-Yu Hu,[a] Keke Jia,[b] Yu Cao,[a] Yan Li,[c] Shan Qin,[a] Fan Zhou,[b] Chen Lin,[a] Dongmei Zhang,[b] and Leyong Wang*[a]

Abstract: Two novel types of supramolecular nanocarriers fabricated by the amphiphilic host–guest inclusion complex formed from water-soluble pillar[6]arene (**WP6**) and azobenzene derivatives **G1** or **G2** have been developed, in which **G1** is structurally similar to **G2** but has an extra phenoxy group in its hydrophobic region. Supramolecular micelles can be initially formed by **WP6** with **G1**, which gradually transform into layered structures with liquid-crystalline properties, whereas stable supramolecular vesicles are obtained from **WP6** and **G2**, which exhibit dual photo- and pH-responsiveness. Notably, the resulting **WP6**⊃**G2** vesicles can efficiently encapsulate anticancer drug mitoxantrone (MTZ) to achieve MTZ-loaded vesicles, which maintain good stability in a simulated normal physiological environment, whereas in an acid environment similar to that of tumor cells or with external UV irradiation, the encapsulated drug is promptly released. More importantly, cytotoxicity assay indicates that such vesicles have good biocompatibility and the MTZ-loaded vesicles exhibit comparable anticancer activity to free MTZ, especially with additional UV stimulus, whereas its cytotoxicity for normal cells was remarkably reduced. Flow cytometric analysis further confirms that the cancer cell death caused by MTZ-loaded vesicles is associated with apoptosis. Therefore, the dual pH- and UV-responsive supramolecular vesicles are a potential platform for controlled release and targeted anticancer drug delivery.

Introduction

Cancer remains one of the world's most devastating diseases, with more than ten million new cases every year.[1] Currently, chemotherapy is still the most commonly used cancer treatment, which also kills healthy cells and causes toxicity to the patient. However, drugs encapsulated in nanocarriers, which are referred to as nanomedicines, have shown therapeutic advantages including better efficacy against resistant tumors and fewer side effects over conventional free drugs.[2] Therefore, it is highly desirable to develop "smart" drug-delivery systems (DDSs) with stimuli-responsiveness, which can either passively or actively target cancer cells. The most recent development in designing responsive nanocarriers has been focused on the micelle- and vesicle-based nanomedicines due to their unique structures, which can efficiently encapsulate the drug and shield it from degradation, increase drug bioavailability, and facilitate the targeted delivery.[2c,3] Up to now, various molecular building blocks have been exploited for the construction of nanocarriers,[4] and among them supramolecular amphiphiles[5] based on noncovalent interactions with stimuli-responsive properties are the most promising ones, since they can not only spontaneously aggregate to form different assemblies, but also undergo structure transitions in response to numerous stimuli, such as pH,[6] temperature,[6b,7] redox,[8] voltage,[9] enzyme,[10] and light.[11] So far, various strategies have been exploited to fabricate stimuli-responsive supramolecular amphiphiles for the construction of nanocarriers;[12] however, to the best of our knowledge, most of the reported responsive nanocarriers only exhibited single stimulus-responsiveness, and there are only a few reports on multistimuli-responsive supramolecular nanocarriers, particularly applied for drug delivery.[6b,13] Therefore, the construction of novel multistimulus-responsive supramolecular drug nanocarriers would be of great interest in the application of biotechnology and biomedicine.

Controllable switching assembly on/off of the nanocarrier is a prerequisite to achieve controlled drug release and its potential applications as a "smart" DDS. Compared with the tradi-

[a] Dr. X.-Y. Hu, Y. Cao, S. Qin, Dr. C. Lin, Prof. Dr. L. Wang
Key Laboratory of Mesoscopic Chemistry of MOE
Center for Multimolecular Organic Chemistry
School of Chemistry and Chemical Engineering
Nanjing University, Nanjing 210093 (China)
E-mail: lywang@nju.edu.cn

[b] K. Jia, F. Zhou, Dr. D. Zhang
State Key Laboratory of Pharmaceutical Biotechnology
School of Life Sciences
Nanjing University, Nanjing 210093 (China)

[c] Dr. Y. Li
State Key Laboratory of Bioelectronics
School of Biological Science and Medical Engineering
Southeast University, Nanjing 210009 (China)

Supporting information for this article is available on the WWW under http://dx.doi.org/10.1002/chem.201405095.

tional polymeric nanocarriers,[14] the supramolecular approach paves an attractive alternative way to construct micelles, vesicles, and other amphiphilic assemblies, since such assemblies are held together by multiple weak and reversible noncovalent interactions, which endow the formed supramolecular nanocarriers with dynamic properties that can be controllably manipulated through the assembly/disassembly processes under external stimuli. Pillararenes,[15] a kind of significant macrocyclic host with unique symmetric pillar architectures and π-rich cavities, have received great attention in constructing various interesting supramolecular systems, including nanomaterials,[16] chemosensors,[17] transmembrane channels,[18] and polymers.[19] So far, although several kinds of noncovalent interactions have been used to fabricate supramolecular amphiphiles, supramolecular nanocarriers constructed by pillararene-based supramolecular amphiphiles have been much less frequently explored in the field of drug delivery.[6a,b] Water-soluble pillar[6]arenes (**WP6**) have been demonstrated to show pH-responsiveness and are significantly biocompatible in aqueous media,[6c] which is of great importance for their applications in drug delivery. In addition, azobenzene derivatives have been confirmed to be especially advantageous for controlling the microscopic structures and relevant functions of various supramolecular systems due to their photoinduced *E*/*Z* isomerization,[11a,20] and the host–guest recognition motif based on the **WP6** and azobenzene motif has been demonstrated to have a strong binding affinity in water driven by hydrophobic and electrostatic interactions.[11b,21] Consequently, we envision that dual photo- and pH-responsive supramolecular nanocarriers could be achieved by designing an appropriate azobenzene-based amphiphilic guest, which could form a supramolecular amphiphile with **WP6** based on the host–guest interaction. The obtained supramolecular amphiphile would possibly be able to form supramolecular micelles or vesicles in water by self-assembly, which could be used as a multiresponsive supramolecular nanocarrier for applications in drug delivery.

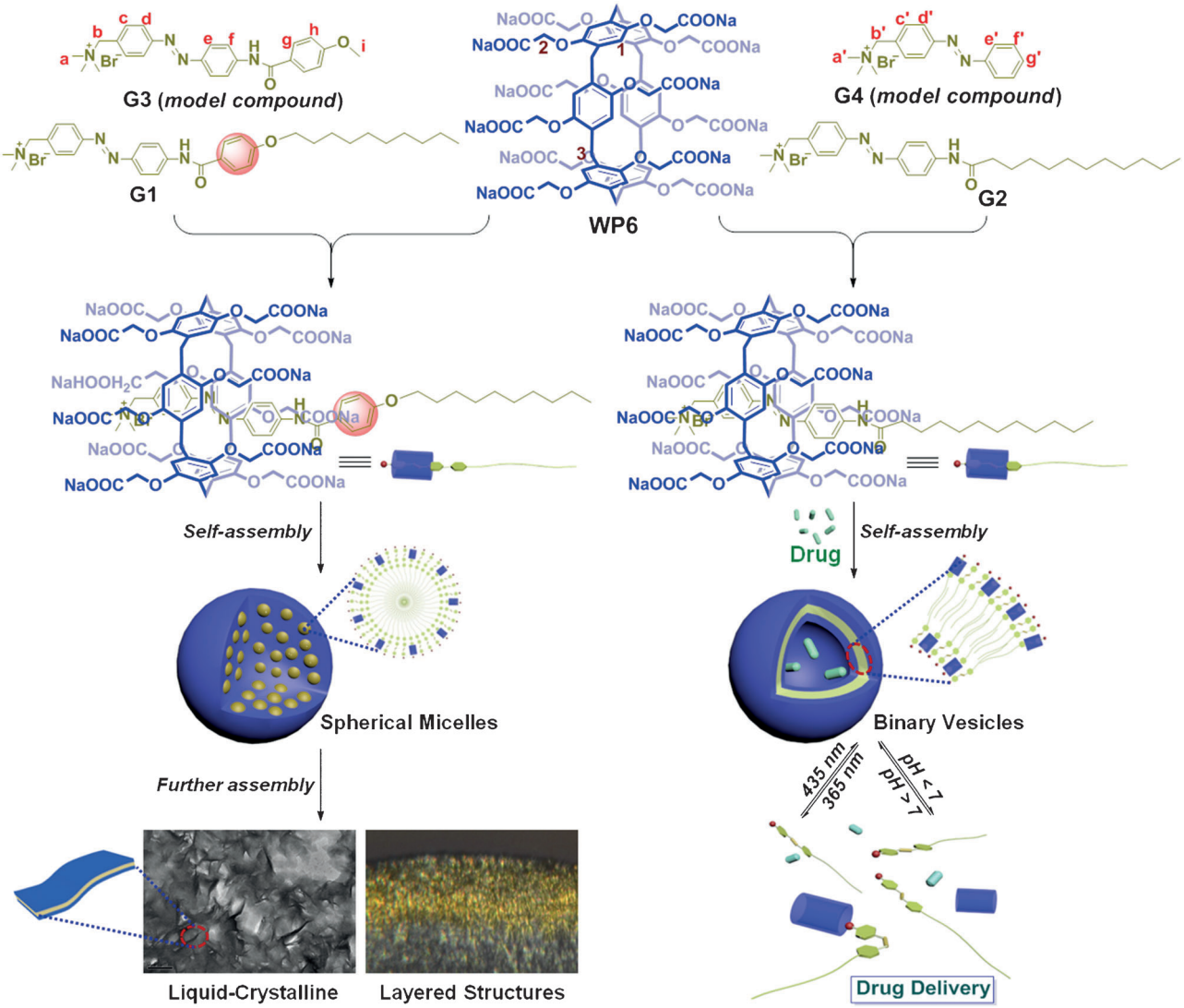

Scheme 1. Schematic illustration of the construction of supramolecular micelles (**WP6⊃G1**) or vesicles (**WP6⊃G2**) and the application of supramolecular vesicles in drug delivery.

Following our recent work on pillararene-based pH- and/or Ca^{2+}-responsive supramolecular vesicles for intracellular drug delivery,[6a,b] herein we report the successful construction of two novel types of pillararene-based supramolecular nanocarriers formed from **WP6** and different azobenzene derivatives, **G1** or **G2**, in which **G1** is structurally similar to **G2** but has an extra phenoxy group in its hydrophobic region (Scheme 1). Supramolecular micelles were initially formed by **WP6** with **G1**, which would gradually be transformed into layered structures with liquid-crystalline properties, probably due to the presence of cooperative intermolecular hydrogen-bonding and π–π interactions within the azobenzene and benzamido motifs of **G1**, whereas stable supramolecular binary vesicles were obtained from **WP6** and **G2**, which exhibited dual photo- and pH-responsiveness. Notably, the resulting **WP6⊃G2** supramolecular vesicles were able to efficiently encapsulate the anticancer drug mitoxantrone (MTZ) to achieve MTZ-loaded vesicles, which showed rapid and efficient MTZ release to an acidic pH environment and/or upon UV stimulus by in vitro drug release experiments. More importantly, cytotoxicity assay demonstrated that the loading of MTZ by **WP6⊃G2** vesicles did not affect the curative effect of MTZ, and the resulting MTZ-loaded supramolecular vesicles exhibited a comparable therapeutic effect for cancer cells to free MTZ, especially with external UV stimulus, whereas the cytotoxicity of MTZ for normal cells was remarkably reduced. Flow cytometric analysis further confirmed that the molecular mechanism for the cancer cell death caused by MTZ-loaded vesicles was associated with apoptosis.

Results and Discussion

Host–guest complexation studies in water

Initially, azobenzene-based amphiphilic molecules **G1** and **G2** were designed, which contained an azobenzene-based quaternary ammonium group as the hydrophilic head and a flexible alkyl phenyl ether segment (**G1**) or alkyl chain (**G2**) as the hydrophobic part as shown in Scheme 1. The **G1** and **G2** exhibit quite poor water solubility, so model guests **G3** and **G4** were used to investigate the host–guest complexation of **WP6⊃G1** and **WP6⊃G2** by ^{1}H NMR, ^{1}H–^{1}H COSY, and 2D ROESY spectroscopy, respectively, in D_2O. From the ^{1}H NMR spectra of **WP6** and **G3** (Figure 1), remarkable upfield chemical shifts of the azobenzene protons (H_c, H_d, H_e, and H_f), methylene protons (H_b), and methyl protons (H_a) of the quaternary ammonium group were observed upon addition of **WP6** due to the shielding effect of the electron-rich cavities of **WP6** toward **G3**. The peaks of protons H_g, H_h, and H_i on **G3** shifted downfield slightly. The above results revealed that **WP6** was fully threaded by guest **G3** with the protons H_a, H_b, H_c, H_d, H_e, and H_f in the hydrophobic **WP6** cavity and other protons H_g, H_h, and H_i out of the cavity. The assignment of these proton signals could be substantiated by the analysis of the ^{1}H–^{1}H COSY data (Figure S2 in the Supporting Information). Moreover, the spatial conformation of such an inclusion complex was further confirmed by the 2D ROESY spectrum (Figure S4 in the Supporting Information), from which intermolecular correlations were ob-

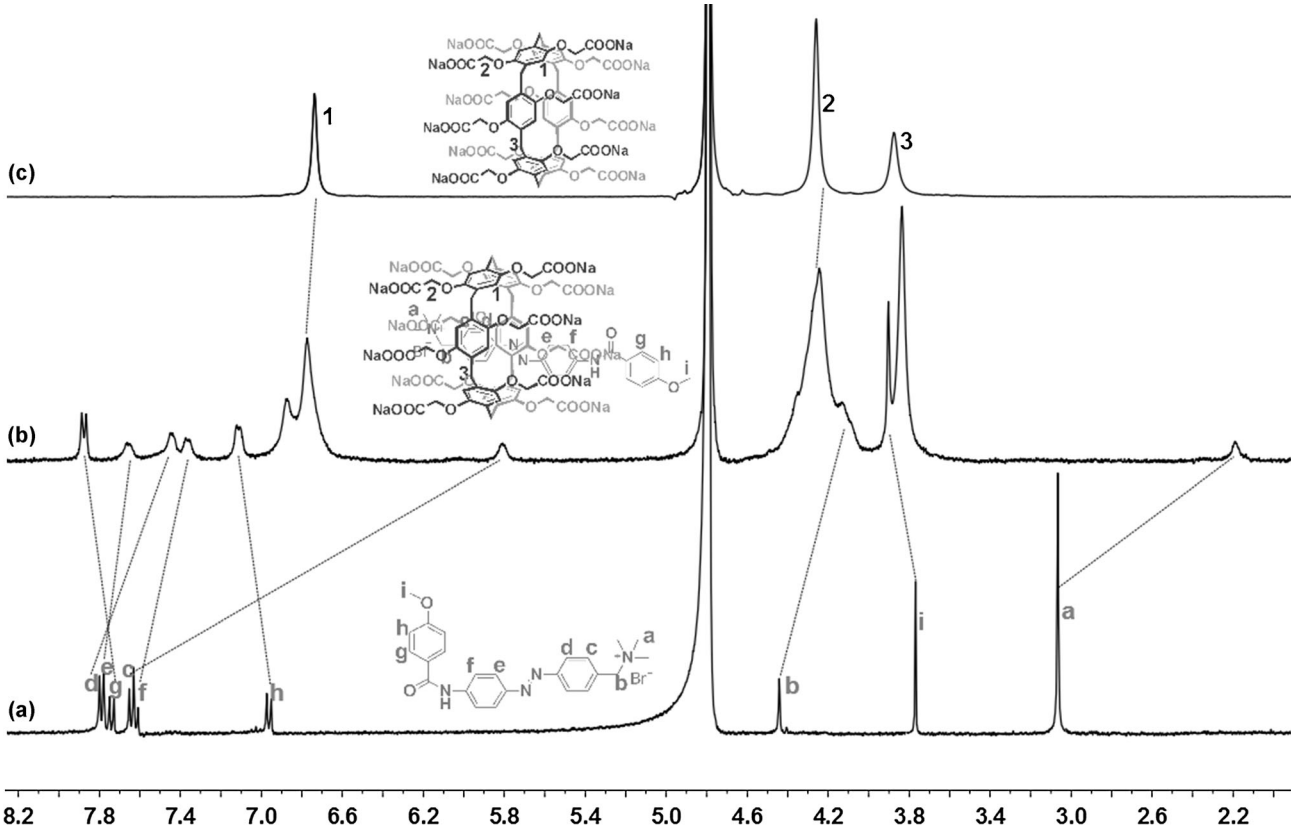

Figure 1. Partial ^{1}H NMR (400 MHz, D_2O, 298 K) spectra: a) model compound **G3** (4.0 mM); b) **G3** (3.0 mM) and **WP6** (6.0 mM); c) **WP6** (6.0 mM).

served between proton H_d on the azobenzene moiety and protons H_1 and H_2 of **WP6**, respectively. The results suggested that the linear model compound **G3** was threaded through the hydrophobic **WP6** cavity to form a [2]pseudorotaxane with its positive azobenzene-based quaternary ammonium head close to the negative carboxylate groups of **WP6**, thereby generating an inclusion complex in the aqueous solution. Similarly, the formation of **WP6⊃G4** inclusion complexes with the positive azobenzene-based quaternary ammonium head of **G4** close to the negative carboxylate groups of **WP6** was also confirmed by NMR spectroscopy (for details see the Supporting Information, Figures S1, S3, and S5).

The stoichiometry of complexation for both **WP6⊃G3** and **WP6⊃G4** in water was further investigated by the Job's plot method using UV/Vis spectroscopy, which confirmed the 1:1 binding stoichiometry for both **WP6⊃G3** and **WP6⊃G4** (Figures S6 and S7 in the Supporting Information). The association constants for **WP6⊃G3** and **WP6⊃G4** in water were determined to be $(1.03\pm0.24)\times10^4\,M^{-1}$ (Figure S8 in the Supporting Information) and $(2.06\pm0.88)\times10^4\,M^{-1}$ (Figure S9 in the Supporting Information), respectively, by using ^1H NMR titration experiments. The binding affinity for such host–guest systems should be attributed to the cooperative electrostatic and hydrophobic interactions. All of the above host–guest investigations indicated that **WP6** formed a "tadpole-like" 1:1 inclusion complex with azobenzene-containing guest **G1** or **G2** as shown in Scheme 1.

Construction of supramolecular nanocarriers in water based on the host–guest complexation of WP6 with G1 or G2

After establishing the above amphiphilic **WP6⊃G1** and **WP6⊃G2** supramolecular complexes, we further investigated the construction of supramolecular nanocarriers from **WP6⊃G1** and **WP6⊃G2** based on their amphiphilic property. Initial investigation of the self-assembly behavior of **G1** and **G2** indicated that both of them could assemble into spherical micellar structures (Figure S12a and S14a in the Supporting Information) with an average diameter of about 37 and 45 nm (Figure S13a and S14b in the Supporting Information), respectively. The critical aggregation concentrations (CACs) for **G1** and **G2** were determined to be 1.49×10^{-4} and 1.33×10^{-4} M, respectively, by using concentration-dependent conductivity measurements (Figures S18a and S19a in the Supporting Information). Notably, when **WP6** (4.35×10^{-6} M) was added to the transparent **G1** (5.0×10^{-5} M) solution (TEM and dynamic light scattering (DLS) confirmed that no micelle was observed), a light blue opalescence and clear Tyndall effect were observed, thus indicating that microaggregates were formed based on the host–guest interactions between **WP6** and **G1**. The size and self-assembly morphology of **WP6⊃G1** aggregates in water were determined by TEM and DLS experiments, which showed that the **WP6⊃G1** complex formed a solid spherical micellar structure (Figure 2a) with an average diameter of about 220 nm (Figure S21a in the Supporting Information).

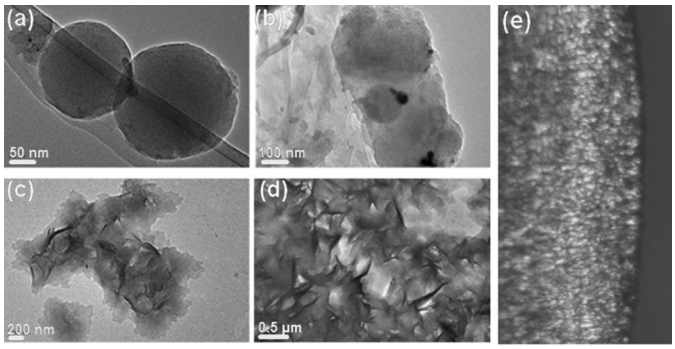

Figure 2. TEM images of spherical micelles formed from **WP6** and **G1** gradually converted to layered structures: the samples prepared after a) 0, b) 3, c) 7, and d) 14 days. e) Representative POM image under crossed polarizers of d). [**WP6**] = 4.35×10^{-6} M and [**G1**] = 5.0×10^{-5} M. Scale bars: a) 50 nm, b) 100 nm, c) 200 nm, d) 0.5 μm.

It was found that adding different amounts of **WP6** to the above **G1** solution led to obvious changes of opalescence intensity in aqueous solution.[6b] Therefore, it was necessary to determine the best molar ratio between **WP6** and **G1** for constructing supramolecular aggregates, which was determined by UV/Vis titration experiments. As shown in Figure 3, upon gradually increasing the amount of **WP6** that was added, the absorbance evolution at 550 nm underwent a sharp increase and then an inverse decrease upon further addition of **WP6**. The rapid increase of the absorbance intensity indicated that **WP6** and **G1** formed a higher-order complex with a tendency toward amphiphilic aggregation, whereas it underwent disassembly upon further addition of **WP6**, generating a simple 1:1 supramolecular inclusion complex. Thus, the best molar ratio of 13.5:1 ([**G1**]/[**WP6**]) for the formation of supramolecular micelles was observed at the inflection point. Based on this best molar ratio, the CAC for **WP6⊃G1** was determined to be 3.28×10^{-6} (Figure S18b in the Supporting Information), which showed a pronounced decrease compared with the CAC value of free **G1** due to the formation of **WP6⊃G1** inclusion complex.

Subsequently, based on ζ-potential experiments, we chose the molar ratio of 11.5:1 ([**G1**]/[**WP6**], ζ-potential = −30.2 mV) for further investigation of its drug-loading property (Figure S15 in the Supporting Information), since under the above conditions, further agglomeration of the obtained supramolecular micelles might not occur due to the repulsive forces-induced increasing stability.[22] Unfortunately, all of the tested hydrophobic anticancer drugs, such as cisplatin, carboplatin, and adriamycin, could not be successfully loaded by such supramolecular micelles. The above problem had puzzled us for a long time until we surprisingly found an interesting phenomenon that such micellar structures were not stable, and gradually converted to supramolecular layered structures with increasing incubation time indicated by their TEM images (Figure 2), which makes them unsuitable as a drug nanocarrier. From the TEM images shown in Figure 2, it was clearly found that the spherical micellar structures became irregular and their boundary became blurred after 3 days (Figure 2b). After

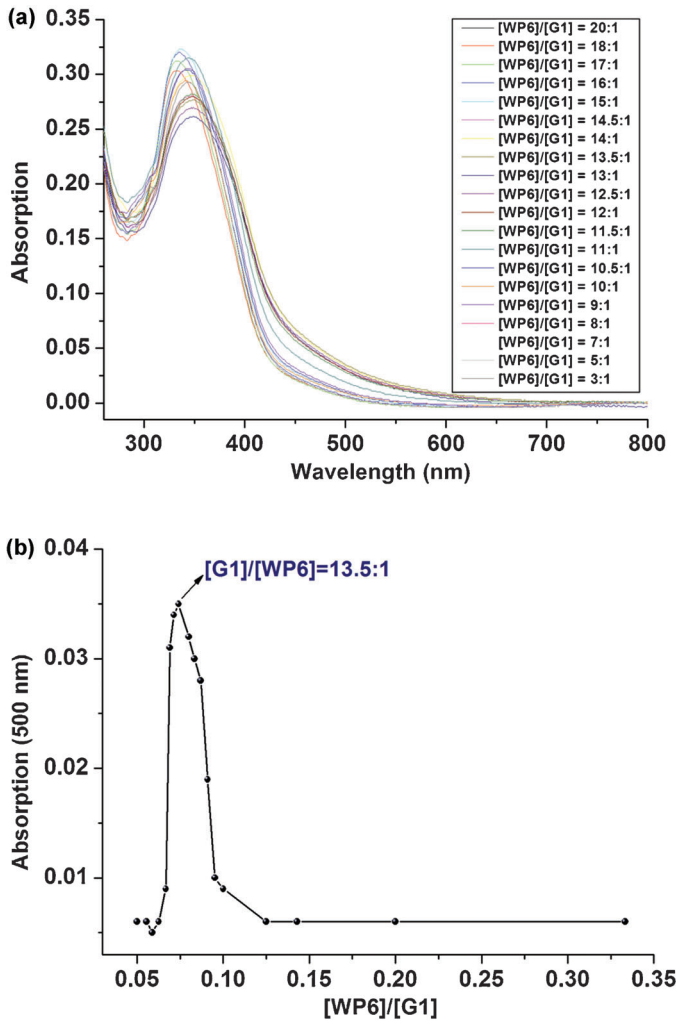

Figure 3. a) UV/Vis absorption of a mixture of **WP6** and **G1** in water with constant **G1** concentration (0.02 mM) on increasing the concentration of **WP6** (0.05–0.33 equiv) at 25 °C. b) Dependence of the relative absorption intensity at 500 nm on the **WP6** concentration with a fixed concentration of **G1** (0.02 mM) at 25 °C.

7 days, there was almost no micellar structure, and only some layer-like structures were observed (Figure 2c). With increasing incubation time, large numbers of layered structures were observed after 14 days (Figure 2d). Moreover, DLS results also demonstrated that the micelles gradually became large aggregates with diameters of approximately 4 to 6 μm (Figure S21 in the Supporting Information). We speculated that such a gradual morphological change, which was similar to that of free **G1** (Figures S12 and S13 in the Supporting Information), might be associated with the liquid-crystalline behavior of **G1**, since the azobenzene motif, especially linking with an extra phenylamide group, has been widely used as a building block to construct various liquid-crystal materials.[23] Further investigation using polarized optical microscopy (POM) suggested that the layered structures formed from **WP6⊃G1** complex exhibited predominantly a mosaic texture (Figure 2e), further suggesting that the above morphological change was associated with the liquid-crystalline property of **G1**. This means that such a supramolecular system might have potential applications for the construction of liquid-crystal materials. We know that it is the cooperative intermolecular hydrogen-bonding and π–π interactions within the azobenzene and benzamido motifs of **G1** that endow it with such unique self-assembly behavior; therefore, we envisaged that the cooperative interactions might be weakened by removing the benzene ring from the hydrophobic region of **G1**, and the designed azobenzene guest **G2** might be suitable to form stable supramolecular nanocarriers with **WP6** by self-assembly.

Along this line, we further investigated whether the established amphiphilic **WP6⊃G2** complex could be used to construct supramolecular nanocarriers. Similar to the above **WP6⊃G1** solution, a clear Tyndall effect could be observed from a mixture of **WP6** (1.11×10^{-5} M) and **G2** (1.0×10^{-4} M) in aqueous solution, which suggested the formation of microaggregates. The best molar ratio of **WP6** and **G2** for such amphiphilic aggregation was determined to be 11:1 ([**G2**]/[**WP6**]) by using similar UV/Vis titration experiments (for details see the Supporting Information, Figure S16). The CAC for **WP6⊃G2** was determined to be 2.52×10^{-6} M (Figure S19b in the Supporting Information), which also showed a pronounced decrease compared with the CAC value of free **G2**. Furthermore, the size and morphology of this nanostructured aggregate formed by **WP6⊃G2** supramolecular amphiphile in aqueous solution are shown in Figure 4 by DLS and TEM measurements, respectively. The DLS results showed that the **WP6⊃G2** complex formed aggregates with a narrow size distribution, giving an average diameter of 160 nm (Figure 4a), and TEM images revealed a hollow spherical morphology with a diameter ranging from 100 to 200 nm, thus indicating convincingly the formation of supramolecular vesicles (Figure 4b), which were different from the micellar structures formed from **WP6⊃G1**. Moreover, the thickness of the hollow vesicles was calculated to be approximately 5 nm from their TEM image (Figure 4c). Considering that the extended length of two molecules of **WP6⊃G2** inclusion complex calculated by Chem3D is about 4.9 nm (Figure S11 in the Supporting Information), the ob-

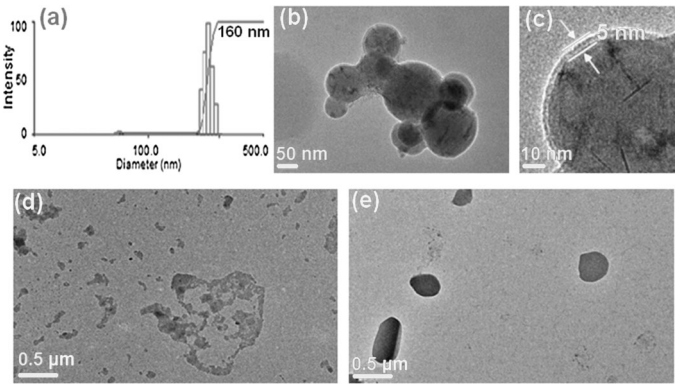

Figure 4. a) DLS data of the **WP6⊃G2** aggregates. b)–e) TEM images: b) **WP6⊃G2** aggregates; c) enlarged image of b); d) **WP6⊃G2** aggregates after the solution pH was adjusted to 6.2; e) **WP6⊃G2** aggregates after the solution pH was adjusted back to 7.4. [**WP6**] = 1.11×10^{-5} M and [**G2**] = 1.0×10^{-4} M.

tained vesicles could possess a bilayer structure with two hydrophilic carboxylate shell layers and one hydrophobic alkyl chain core layer as shown in Scheme 1. In addition, ζ-potential experiments were also performed to examine the stability of the obtained vesicles with different **G2**/**WP6** molar ratios (Figure S17 in the Supporting Information). The results suggested that the ζ-potential of the obtained vesicles changed gradually from positive (28.5 mV, [**G2**]/[**WP6**] = 12:1) to negative (−59.1 mV, [**G2**]/[**WP6**] = 9:1) upon the addition of **WP6**. In particular, the ζ-potential of the vesicles formed at the best molar fraction ([**G2**]/[**WP6**] = 11:1) was close to 0 mV, which means that the vesicles obtained at the best molar ratio were not stable due to the absence of repulsive forces among vesicles. Therefore, considering the repulsive forces-induced increasing stability of vesicles,[22] a molar ratio of 9:1 ([**G2**]/[**WP6**], ζ-potential = −59.1) was chosen for further investigation of their stimuli-responsive behavior as well as their application in drug delivery.

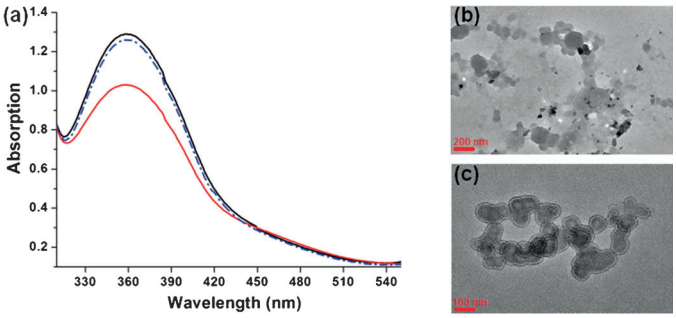

Figure 5. a) UV/Vis spectra of the vesicular solution of **WP6⊃G2** [initial (black line) and after irradiation with UV light at 365 nm for 15 min (red line), and then after irradiation with visible light at 435 nm for 15 min (blue line)]. [**WP6**] = 1.11×10^{-5} M and [**G2**] = 1.0×10^{-4} M). b) **WP6⊃G2** aggregates after irradiation with UV light at 365 nm for 15 min; c) **WP6⊃G2** aggregates after irradiation with UV light at 365 nm, and then further irradiation with visible light at 435 nm for 15 min.

Photo- and pH-responsiveness of the WP6⊃G2 supramolecular vesicles

The multistimulus-responsive properties of supramolecular vesicles are of extreme importance for their applications in DDSs.[24] Compound **WP6** has been demonstrated to show pH-responsiveness in aqueous solution,[6a] and the azobenzene motif is a perfect photoresponsive building block for the construction of various photoresponsive supramolecular systems.[11a,25] As expected, the Tyndall effect for **WP6⊃G2** solution disappeared after adjusting the solution pH to 6.2; meanwhile, no vesicle was observed in the TEM image (Figure 4d) due to the precipitation of **WP6** as its acid form out of the acidic aqueous solution. Moreover, when the pH value of the above solution was adjusted back to 7.4, vesicle re-formation was observed (Figure 4e), which was also verified by DLS experiment (Figure S22b in the Supporting Information), clearly confirming the pH-responsive behavior of the **WP6⊃G2** vesicles due to the reversible assembly/disassembly process of the amphiphilic host–guest complex.

Besides the pH-responsiveness, more importantly, these obtained **WP6⊃G2** supramolecular vesicles exhibited good photoresponsive properties due to the UV-induced *E*/*Z* isomerization of **G2**. As shown in Figure 5a, upon irradiation of the **WP6⊃G2** vesicular solution with UV light at 365 nm, the absorption band at around 360 nm decreased remarkably, thus indicating the photoisomerization of the *trans*-**G2** to the *cis*-**G2** state induced by UV irradiation. Conversely, upon further irradiation of the above solution with visible light at 435 nm, the absorption peak at 360 nm attributable to *trans*-**G2** increased to almost its original intensity, which suggests a reversible change from the *cis* to the *trans* form; such reversible transformation was also supported by a ^{1}H NMR spectroscopic study (Figure S10 in the Supporting Information). Furthermore, the TEM images showed that when the **WP6⊃G2** vesicular solution was irradiated with UV light, most of the vesicles collapsed and only a few irregular aggregates could be observed (Figure 5b). On the contrary, upon further irradiation of the above solution with visible light at 435 nm, large numbers of vesicles were observed again (Figure 5c), which was also supported by DLS experiments (Figure S22c in the Supporting Information). All the above results clearly demonstrated that such **WP6⊃G2** supramolecular vesicles exhibited good pH- and UV-responsiveness, which endows them with the ability to encapsulate substrates under neutral conditions and release them in response to acidic conditions or upon UV stimulation.

Encapsulation of hydrophilic drug MTZ by WP6⊃G2 vesicles and its photo- and pH-responsive in vitro release

The hollow vesicles prefer to load hydrophilic drugs, so MTZ, a chemotherapy drug that is widely used to treat a broad range of solid malignant tumors,[26] was chosen as a model drug to investigate the encapsulation efficiency of **WP6⊃G2** vesicles as well as their release behavior upon external stimulation. Compared with the pale yellow **WP6⊃G2** vesicular solution, the MTZ-loaded vesicular solution turned light blue after removing the excess unloaded MTZ molecules by dialysis, which indicated that MTZ was successfully encapsulated into the **WP6⊃G2** vesicle cavities (Figure 6a). Meanwhile, the UV absorption of MTZ-loaded vesicular solution became much stronger from 580 to 660 nm than for the unloaded vesicular solution (Figure 6b), which represents the characteristic absorption of MTZ in aqueous solution. Moreover, DLS results (Figure 6c) and the TEM image (Figure 6d) showed that MTZ-loaded vesicles were much larger in size (≈364 nm) than the unloaded vesicles (≈160 nm), which further confirmed that MTZ molecules were successfully loaded into the vesicle cavities. Based on the UV/Vis absorption spectra, the MTZ encapsulation efficiency was calculated to be 76%, thus indicating that such supramolecular vesicles have a very efficient drug-loading capability.[9,10]

Subsequently, the release behavior of MTZ-loaded supramolecular vesicles was investigated under an acidic pH environment and/or upon UV stimulation. As shown in Figure 7a, under simulated physiological conditions (pH 7.4), the cumulative leakage of MTZ from MTZ-loaded vesicles was less than

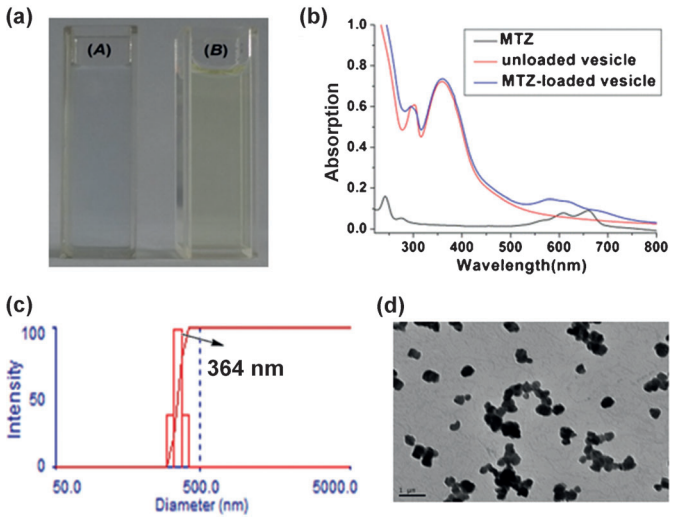

Figure 6. a) Color change of MTZ-loaded vesicles (*A*) compared with unloaded vesicles (*B*). b) UV/Vis absorption spectra of the solution of MTZ, unloaded vesicles, and MTZ-loaded vesicles at 25 °C in water. c) DLS data of MTZ-loaded vesicles. d) TEM image of MTZ-loaded vesicles.

8% within 12 h. However, when the solution pH was adjusted to acidity, MTZ was released in significant amounts with a cumulative release amount of 44% at pH 6.2 and 93% at pH 4.4 within 12 h. In particular, rapid MTZ release was observed in the first 2 h from the profiles. The microenvironment of tumor cells is acidic due to the presence of excessive lactic acid and CO_2 as metabolites, so the rapid release of MTZ from MTZ-loaded vesicles can be selectively triggered in tumor tissues, which is extremely significant for specific targeted therapy, shortening the administration time and greatly increasing the curative effect.[27] On the other hand, when the MTZ-loaded vesicular solution was irradiated with UV light, the absorption peak at around 360 nm attributable to *trans*-**G2** decreased dramatically, whereas the absorption band at 660 nm corresponding to the characteristic absorption of MTZ gradually increased with the irradiation time (Figure 7b). This suggested the gradual disassembly of vesicles due to the configuration change of *trans*-**G2** to *cis*-**G2**, which resulted in the gradual release of MTZ from MTZ-loaded vesicles, and the cumulative amount of released drug was about 60% after 4 h (Figure 7c).

Thereafter, the dual pH-/UV-responsive properties of MTZ-loaded vesicles were also investigated. When low pH and UV irradiation were simultaneously exerted on the MTZ-loaded vesicles, a burst release of MTZ was observed during the initial first hour because of the quick disaggregation of vesicles, and the cumulative amount of released drug was up to 100% (pH 4.4) and 74% (pH 6.2) after 4 h (Figure 7d). This is consistent with the results of acid-stimulated precipitation of **WP6** as its acid form and photoinduced disassembly of the supramolecular vesicles. Overall, these results showed that such

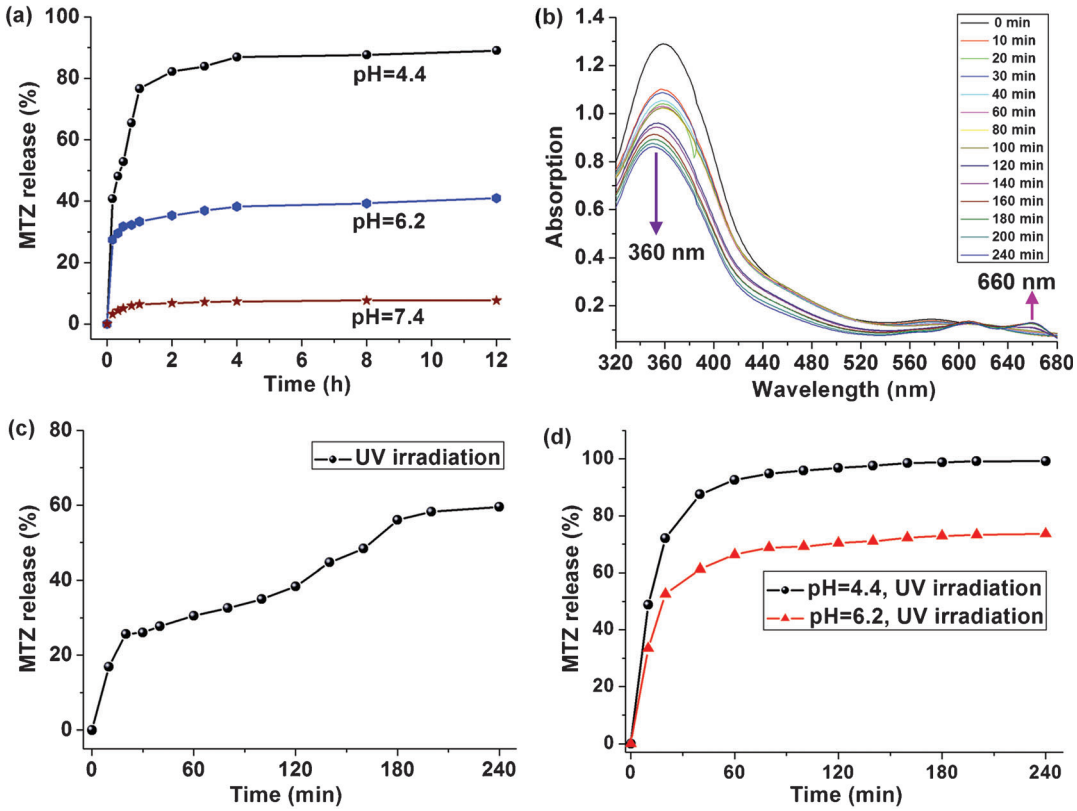

Figure 7. a) pH-responsive MTZ release profiles of MTZ-loaded vesicles in release media with different pH values. b) UV/Vis absorption spectra of the solution of MTZ-loaded vesicles in water (pH 7.4) after irradiation with UV light at 365 nm for different times (0–240 min). c) Release of MTZ from MTZ-loaded vesicles in water (pH 7.4) after irradiation with UV light at 365 nm for different times (0–240 min). d) Dual pH-/UV-responsive MTZ release profiles of MTZ-loaded vesicles.

MTZ-loaded vesicles were able to realize a quick and efficient release of the encapsulated drugs when they were synchronously triggered by low pH and UV light.

Cytotoxicity and anticancer efficiency of MTZ-loaded vesicles

Subsequent stability investigations of the **WP6⊃G2** vesicles in phosphate-buffered saline (PBS) or under physiological conditions, such as 150 mM NaCl solution and 10% serum, showed that the cumulative leakage of MTZ from MTZ-loaded vesicles was less than 5% within 48 h in PBS buffer or 10% serum. Even in the hypertonic NaCl solution (150 mM), the cumulative leakage of MTZ from MTZ-loaded vesicles was only about 7% within 48 h (Figure 8), which indicated that MTZ-loaded vesicles have good stability under physiological conditions and they are ideal candidates for DDSs. Moreover, as DDS materials, the biocompatibility of the carrier is also a key index for its biomedical application. Compound **WP6** has been demonstrated to be significantly biocompatible in aqueous media, and therefore the cytotoxicity of guest **G2** and unloaded vesicles was evaluated by the MTT method against NIH3T3 normal cells. Figure 9a shows the cell viability after 24 h of incubation with **G2** or unloaded vesicles at a concentration varying from 5 to 100 μM. Clearly, the cell viability remains above 80% even when the concentration of **G2** or unloaded vesicles increases to 100 μM. Consequently, **WP6⊃G2** supramolecular vesicles that have good biocompatibility are a suitable material for DDSs. In addition, it was found that the relative viability of NIH3T3 cells incubated with MTZ-loaded vesicles was always much higher than that in the free MTZ from 48 to 96 h ($p < 0.05$, Figure 9b). Also, the morphology of living cells in the MTZ-loaded vesicle groups was better than that in the free MTZ after 96 h (Figure 10), which indicated that the toxicity of MTZ was remarkably reduced upon its encapsulation by the **WP6⊃G2** vesicles.

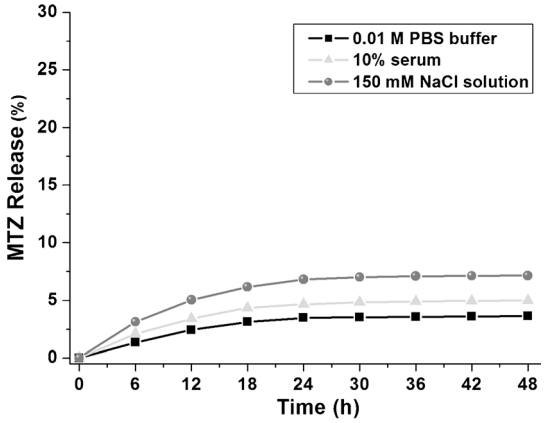

Figure 8. Stability of the MTZ-loaded **WP6⊃G2** vesicles in PBS buffer (pH 7.4), 150 mM NaCl solution, and 10% serum at 37 °C (0–48 h, vesicles were prepared in 0.01 M PBS buffer).

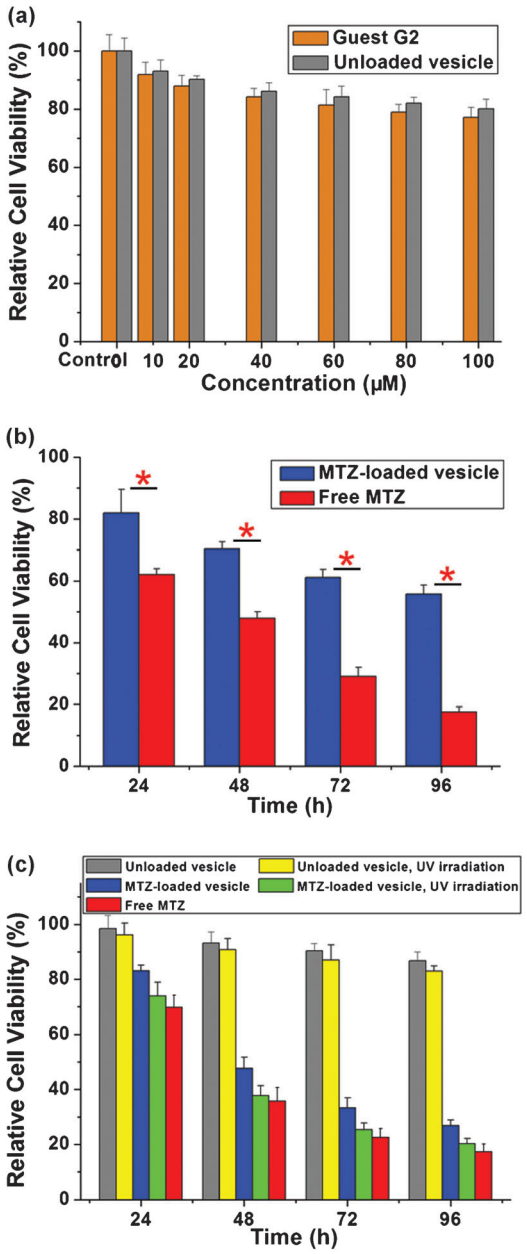

Figure 9. a) In vitro cytotoxicity of guest **G2** and unloaded vesicles against NIH3T3 cells after 24 h of incubation. b) Effect of MTZ-loaded vesicles and free MTZ on the viability of NIH3T3 cells at different times. c) Anticancer activity of unloaded vesicles, MTZ-loaded vesicles, and free MTZ with or without UV irradiation against MCF-7 cells at different times. Statistically significant differences were observed ($p < 0.05$) (*).

Moreover, the anticancer activity of MTZ-loaded vesicles with or without UV irradiation was also investigated by MTT assay against MCF-7 cancer cells, for which the unloaded vesicles and free MTZ were used as controls. As shown in Figure 9c, it was found that the relative cell viability of the MTZ-loaded vesicle group against cancer cells with UV irradiation was only 20% after 96 h, which showed similar therapeutic effects to the free MTZ group (17%), whereas that without irradiation was about 27% (Figure 9c), which indicated that additional UV stimulation facilitated drug release compared with the single pH stimulus. Additionally, for the unloaded vesicle group, the cell viability without UV irradiation retained about

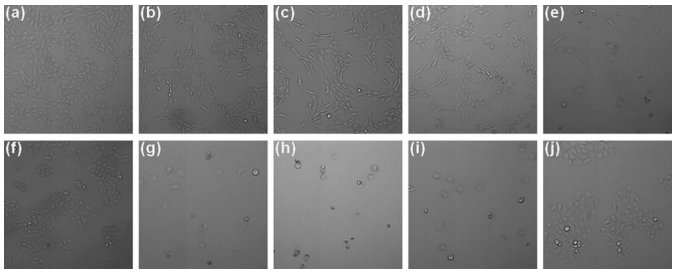

Figure 10. Images of living NIH3T3 cells in a) blank, b) **G2**, c) unloaded vesicle, d) MTZ-loaded vesicle, and e) MTZ groups after 96 h. Images of living MCF-7 cells in f) blank, g) MTZ, h) MTZ-loaded vesicle, i) MTZ-loaded vesicle with UV irradiation, and j) unloaded vesicle with UV irradiation groups after 96 h.

86%, and only a slight decrease (4%) was found after irradiation, thus indicating that the effect of irradiation was negligible, which could also be observed from the morphology of living cells (Figure 10). All of the above results implied that loading of MTZ by **WP6⊃G2** vesicles reduced its cytotoxicity for normal cells but kept the therapeutic effect of MTZ for cancer cells, especially with external UV stimulus. A rational explanation is that compared with normal cells, tumor cells have strong phagocytosis and an acidic microenvironment to cause the disassembly of MTZ-loaded vesicles to release MTZ, especially with external UV stimulus.[28] Therefore, such supramolecular vesicles based on the host–guest complexation of **WP6** and azobenzene derivatives are promising DDSs.

Cell apoptosis

To further understand the molecular mechanism of the therapeutic effect of MTZ-loaded vesicles on cancer cells, flow cytometric analysis based on the fluorescein isothiocyanate (FITC)-Annexin V/propidium iodide (PI) method was used to investigate whether the antitumor effect of MTZ-loaded vesicles was associated with apoptosis. MCF-7 cells were incubated with MTZ-loaded vesicles for 48 and 96 h, and then they were subjected to FITC-Annexin V/PI staining. The cells without treatment by MTZ-loaded vesicles were used as control. After incubating with MTZ-loaded vesicles for 48 h, the quantity of apoptotic cells of the whole tested MCF-7 cells was about 47.2%, and the early apoptotic cells took a percentage of 37.5% (Figure 11). When the incubation time was extended to 96 h, the ratio of apoptotic cells significantly increased to 70.2%, and the majority of apoptotic cells were still the early apoptotic cells (Figure 11). Therefore, the above flow cytometry data demonstrated that MTZ-loaded vesicles could induce apoptosis in MCF-7 cells and the apoptosis effect was time-dependent.

Conclusion

Two novel types of pillararene-based supramolecular nanocarriers were successfully constructed from an amphiphilic host–guest inclusion complex in water: 1) supramolecular micelles were formed from **WP6** and azobenzene guest **G1**, which gradually transformed into layered structures with liquid-crystalline properties, probably due to the presence of cooperative intermolecular hydrogen-bonding and π–π interactions within the azobenzene and benzamido motifs of **G1**; and 2) stable supramolecular vesicles were obtained from **WP6** and **G2**, which displayed a significant dual photo- and pH-responsive behavior. Significantly, drug loading and in vitro release experiments demonstrated that MTZ could be successfully encapsulated into the **WP6⊃G2** supramolecular vesicles, and the resulting MTZ-loaded vesicles exhibited an excellent responsiveness and rapid release of the encapsulated MTZ in an acid environment similar to that of tumor cells or with external UV irradiation; in a simulated normal physiological environment, such supramolecular vesicles maintain good stability. More importantly, cytotoxicity tests and flow cytometric analysis further demonstrated that the loading of MTZ by **WP6⊃G2** supramolecular vesicles did not affect the therapeutic effect of MTZ on cancer cells, especially with additional UV stimulus, whereas its cytotoxicity for normal cells was remarkably reduced, and the cancer cell death caused by MTZ-loaded vesicles was associated with apoptosis. The present supramolecular vesicle system with dual pH- and UV-responsiveness is expected to have great potential applications for the development of "smart" drug-delivery systems. The anticancer activity of such MTZ-loaded vesicles against a human melanoma cell line and

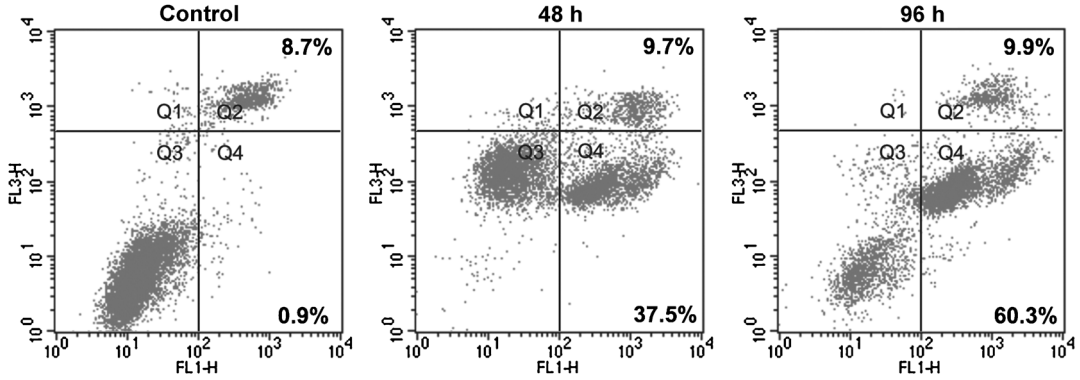

Figure 11. Flow cytometric analysis of MCF-7 cells treated with MTZ-loaded vesicles (0.94 μM) after incubation for different times. Q1, necrotic cells; Q2, late apoptotic cells; Q3, living cells; Q4, early apoptotic cells. Inserted numbers in the profiles indicate the percentage of the cells present in this area.

animal testing are in progress in our laboratory to investigate their potential application for the therapy of skin carcinoma.

Experimental Section

Materials

Mitoxantrone (MTZ; >98%) was provided by Melone Pharma (Dalian, China). Tetrachloromethane (CCl_4), dichloromethane (CH_2Cl_2), and acetonitrile (CH_3CN) were dried according to procedures described in the literature, and other solvents were used as received without further purification unless otherwise stated. Column chromatography was performed with silica gel (200–300 mesh) produced by Qingdao Marine Chemical Factory, Qingdao (China). All the other chemicals were purchased from commercial suppliers, were of analytical grade, and used without further purification.

Measurements

NMR spectra were recorded on a Bruker DPX 300 MHz spectrometer (or Bruker DPX 400 MHz spectrometer) with internal standard tetramethylsilane (TMS) and solvent signals as internal references at 25 °C, and the chemical shifts (δ) were expressed in ppm and *J* values given in Hertz. Low-resolution electrospray ionization mass spectrometry (LR-ESI-MS) was performed on Finnigan Mat TSQ 7000 instruments. High-resolution electrospray ionization mass spectrometry (HR-ESI-MS) was performed on an Agilent 6540 Q-TOF LC/MS system equipped with an ESI probe operating in positive-ion mode with direct infusion. UV/Vis spectra were recorded in a quartz cell (light path 10 mm) on a PerkinElmer Lambda 35 UV/Vis spectrometer. The critical aggregation concentration (CAC) determination of **G1**, **WP6⊃G1**, **G2**, and **WP6⊃G2** was carried out on a DDS-307A instrument according to procedures reported in the literature.[6c] TEM images were recorded on a JEM-2100 instrument. Samples were prepared by dropping the solution onto a carbon-coated copper grid. DLS measurements were performed with a Brookhaven BI-9000AT system (Brookhaven Instruments Corporation, USA) equipped with a 200 mW laser light and operating at $\lambda = 514$ nm. ζ-potential measurement was performed at 25 °C on a Zetasizer Nano Z apparatus (Malvern Instruments Ltd., UK) using the Smoluchowski model for the calculation of the ζ-potential from the measured electrophoretic mobility.

Synthetic procedures

All reactions were performed under an ambient atmosphere unless otherwise stated. Compound **WP6** was synthesized and purified according to previously reported procedures (Scheme S1 in the Supporting Information).[12f] The detailed synthetic procedures for azobenzene derivatives (**G1** and **G2**) are shown in Scheme 2, and the synthetic routes of the model compounds (**G3** and **G4**) are shown in Scheme S2 in the Supporting Information.

Synthesis of compound 1: Ethyl 4-hydroxybenzoate (3.32 g, 20 mmol) was dissolved in CH_3CN (200 mL), K_2CO_3 (16.6 g, 120 mmol) and 1-bromodecane (6.64 g, 30 mmol) were added to the above solution, and then the reaction mixture was stirred at reflux temperature overnight. After filtering, the solvent was re-

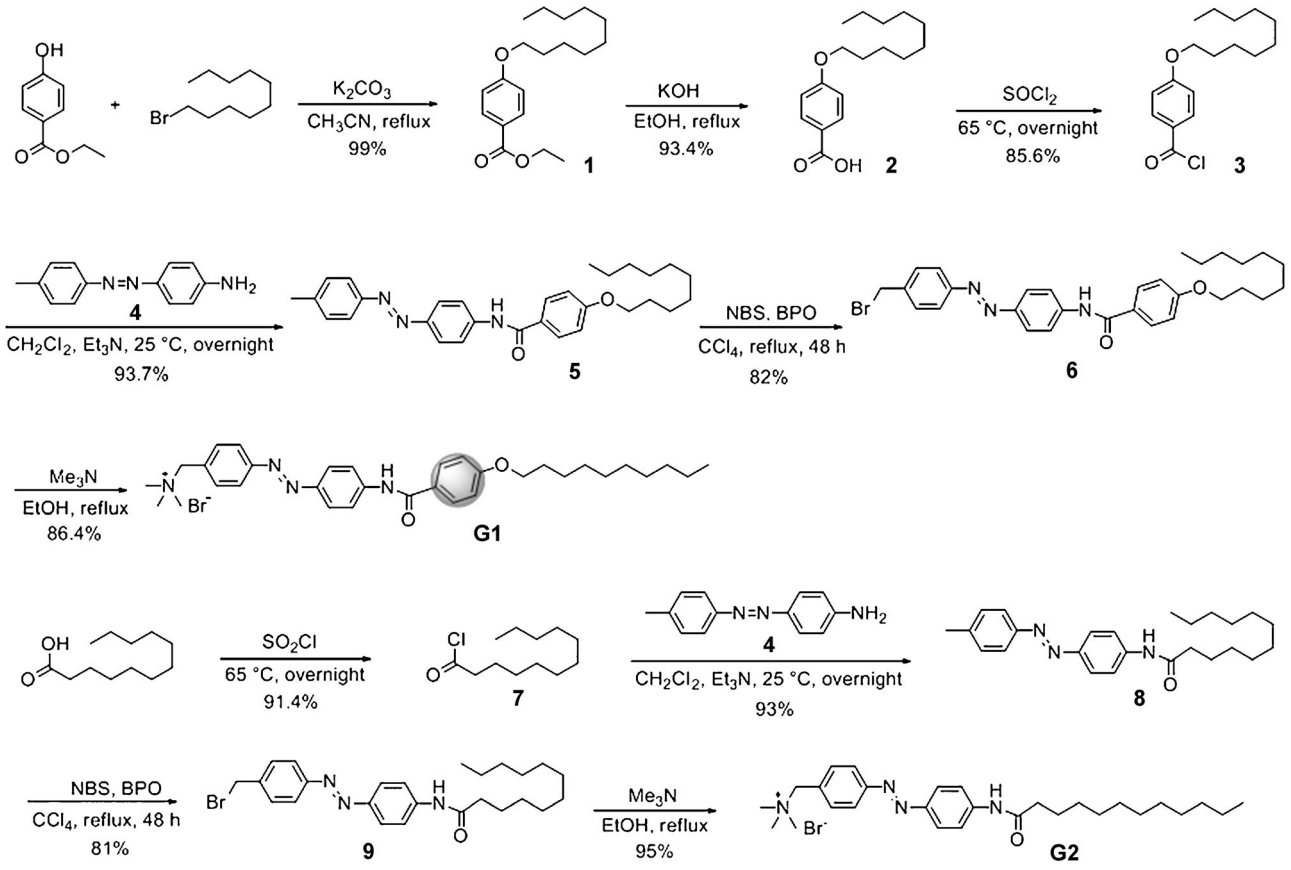

Scheme 2. Synthesis of the azobenzene derivatives **G1** and **G2**. NBS = *N*-bromosuccinimide, BPO = benzoyl peroxide.

moved under vacuum to give the crude product. Column chromatography was used in the final separation with hexane/CH_2Cl_2 (20:1–1:1, v/v) as the eluent, to give compound **1** as a colorless oil (6.1 g, 19.9 mmol, 99%). ^{1}H NMR (300 MHz, $CDCl_3$): δ = 8.01–7.96 (m, 2H), 6.92–6.87 (m, 2H), 4.34 (q, J = 7.1 Hz, 2H), 4.00 (t, J = 6.6 Hz, 2H), 1.85–1.73 (m, 2H), 1.56–1.15 (m, 18H), 0.88 ppm (t, J = 6.7 Hz, 3H).

Synthesis of compound 2: Compound **1** (3.06 g, 10 mmol) was dissolved in EtOH (50 mL) and KOH (3.37 g, 60 mmol) was dissolved in water (5 mL), then the KOH solution was added to the solution of compound **1** and the reaction mixture was stirred at reflux temperature for 2 h. After the reaction was completed, the reaction mixture was poured into water (100 mL) and CH_2Cl_2 (100 mL) was added, then the pH of the solution was adjusted to 3.0 by using concentrated hydrochloric acid (37%). The organic layer was separated and dried over Na_2SO_4. After removing the solvent under vacuum, the product **2** was obtained as a colorless oil (2.6 g, 9.34 mmol, 93.4%). ^{1}H NMR (300 MHz, $CDCl_3$): δ = 11.01 (br s, 1H), 8.05 (d, J = 8.8 Hz, 2H), 6.92 (d, J = 8.8 Hz, 2H), 4.01 (t, J = 6.5 Hz, 2H), 1.86–1.73 (m, 2H), 1.46–1.43 (m, 2H), 1.27 (s, 13H), 0.88 ppm (t, J = 6.0 Hz, 3H).

Synthesis of compound 3: Compound **2** (2.6 g, 9.32 mmol) was suspended in thionyl chloride ($SOCl_2$, 6.6 mL). Then the mixture was stirred at 65 °C overnight. After evaporating the excess thionyl chloride, the crude product **3** was obtained as a colorless oil (2.37 g, 7.98 mmol, 85.6%).

Synthesis of compound 5: Compound **4**[29] (1.06 g, 5.0 mmol) was dissolved in dry CH_2Cl_2 (30 mL) and Et_3N (0.76 g, 7.5 mmol) was added to the solution. Compound **3** (2.23 g, 7.5 mmol) was dissolved in dry CH_2Cl_2 (5 mL) and then it was added dropwise to the above solution of **4** in 30 min. After stirring overnight at 25 °C, the solvent was removed under vacuum to give a yellow solid. Column chromatography was used in the final separation with petroleum ether/CH_2Cl_2 (20:1, v/v) as the eluent, to give yellow solid compound **5** (2.21 g, 4.69 mmol, 93.7%). ^{1}H NMR (300 MHz, [D$_6$]DMSO): δ = 10.40 (s, 1H), 8.00 (dd, J = 12.6, 8.9 Hz, 4H), 7.90 (d, J = 8.9 Hz, 2H), 7.79 (d, J = 8.3 Hz, 2H), 7.40 (d, J = 8.3 Hz, 2H), 7.07 (d, J = 8.8 Hz, 2H), 4.06 (t, J = 6.5 Hz, 2H), 2.41 (s, 3H), 1.80–1.67 (m, 2H), 1.43–1.26 (m, 14H), 0.86 ppm (t, J = 6.6 Hz, 3H); ^{1}H NMR (300 MHz, $CDCl_3$): δ = 7.94 (d, J = 8.6 Hz, 3H), 7.87–7.77 (m, 5H), 7.30 (d, J = 8.1 Hz, 2H), 6.97 (d, J = 8.7 Hz, 2H), 4.02 (t, J = 6.5 Hz, 2H), 2.43 (s, 3H), 1.87–1.74 (m, 2H), 1.52–1.40 (m, 2H), 1.28–1.25 (m, 12H), 0.88 ppm (t, J = 6.4 Hz, 3H); ^{13}C NMR (75 MHz, $CDCl_3$): δ = 165.2, 162.4, 141.3, 140.5, 129.7, 128.9, 126.5, 123.9, 122.8, 120.0, 114.6, 68.3, 31.9, 29.7, 29.6, 29.4, 29.3, 29.1, 26.0, 22.7, 21.5, 14.1 ppm; ESI-MS: m/z (%): 472.30 [M+ H]$^+$; HR-ESI-MS: m/z calcd for [M+H]$^+$ $C_{30}H_{38}N_3O_2$: 472.2964; found: 472.2966; [M+Na]$^+$ $C_{30}H_{37}N_3O_2Na$: 494.2784; found: 494.2788.

Synthesis of compound 6: Compound **5** (236 mg, 0.5 mmol), NBS (143 mg, 0.55 mmol), and BPO (4.6 mg, 0.09 mmol) were dissolved in CCl_4 (5 mL) under an argon atmosphere, then the reaction mixture was heated at reflux for 24 h. When ^{1}H NMR spectroscopy indicated the reaction was completed, the mixture was cooled to 0 °C and filtered under vacuum to give a yellow powder, which was washed with cold CH_2Cl_2 (3×20 mL). Finally, the desired compound **6** was obtained as a mixture with a small amount of the starting material compound **5** (0.17 g). The two compounds have the same R_f value based on TLC, which was confirmed by the ^{1}H NMR spectrum (Figure S27 in the Supporting Information).

Synthesis of azobenzene derivative G1: A solution of compound **6** (165 mg, also having a small amount of compound **5**) in ethanol (3.0 mL) and Me_3N (30% in water, 1.0 mL) was stirred at reflux temperature for 24 h. The solution was concentrated under reduced pressure. The residue was diluted with chloroform (20.0 mL), the orange precipitate was collected by filtration and washed with CH_2Cl_2 to remove **5**, and the target product **G1** was obtained as an orange solid (158 mg, about 86.4%). ^{1}H NMR (300 MHz, CD_3OD): δ = 8.10–7.88 (m, 8H), 7.75 (d, J = 8.1 Hz, 2H), 7.05 (d, J = 8.8 Hz, 2H), 4.63 (s, 2H), 4.08 (t, J = 6.4 Hz, 2H), 3.17 (s, 9H), 1.87–1.76 (m, 2H), 1.51 (br s, 2H), 1.32 (br s, 12H), 0.90 ppm (t, J = 6.0 Hz, 3H); ^{13}C NMR (75 MHz, CD_3OD): δ = 167.1, 162.5, 153.9, 148.6, 142.6, 133.7, 129.6, 129.4, 126.3, 123.7, 122.9, 122.0, 120.6, 114.0, 68.7, 68.0, 51.9, 31.7, 29.3, 29.3, 29.1, 29.1, 28.9, 25.8, 22.4, 13.1 ppm; ESI-MS: m/z (%): 529.40 [M−Br]$^+$; HR-ESI-MS: m/z calcd for [M−Br]$^+$ $C_{33}H_{45}N_4O_2$: 529.3537; found: 529.3542.

Synthesis of compound 7: Dodecanoic acid (2.0 g, 10 mmol) was suspended in thionyl chloride ($SOCl_2$, 8 mL), then the mixture was stirred at 65 °C overnight. After evaporating the excess thionyl chloride, the crude product **7** was obtained as a colorless oil (2.0 g, 9.14 mmol, 91.4%).

Synthesis of compound 8: Compound **4**[29] (0.62 g, 2.9 mmol) was dissolved in dry CH_2Cl_2 (15 mL) and Et_3N (0.59 g, 5.8 mmol) was added to the solution. Compound **7** (0.97 g, 4.4 mmol) was dissolved in dry CH_2Cl_2 (5 mL) and then it was added dropwise to the above solution of compound **4**. After stirring overnight at 25 °C, the solvent was removed under vacuum to give a yellow solid. Column chromatography was used in the final separation with petroleum ether/CH_2Cl_2 (1:1, v/v) as the eluent, to give a yellow solid **8** (1.61 g, 4.09 mmol, 93%). ^{1}H NMR (300 MHz, $CDCl_3$): δ = 7.92 (d, J = 8.8 Hz, 2H), 7.82 (d, J = 8.3 Hz, 2H), 7.70 (d, J = 8.7 Hz, 2H), 7.43 (s, 1H), 7.30 (d, J = 8.2 Hz, 2H), 2.43 (s, 3H), 2.42–2.34 (m, 2H), 1.81–1.67 (m, 2H), 1.44–1.17 (m, 16H), 0.88 ppm (t, J = 6.7 Hz, 3H); ^{13}C NMR (75 MHz, $CDCl_3$): δ = 171.6, 150.5, 148.8, 141.4, 140.5, 129.8, 124.1, 122.8, 119.7, 38.0, 31.9, 29.6, 29.5, 29.4, 29.4, 29.3, 25.6, 22.7, 21.5, 14.1 ppm; ESI-MS: m/z (%): 394.25 [M+H]$^+$; HR-ESI-MS: m/z calcd for [M+H]$^+$ $C_{25}H_{36}N_3O$: 394.2858; found: 394.2861; [M+Na]$^+$ $C_{25}H_{35}N_3ONa$: 416.2678; found: 416.2683.

Synthesis of compound 9: Compound **8** (0.5 g, 1.27 mmol), NBS (0.34 g, 1.9 mmol), and BPO (15 mg, 0.064 mmol) were dissolved in CCl_4 (15 mL) under an argon atmosphere, then the reaction mixture was heated at reflux for 48 h. When ^{1}H NMR spectroscopy indicated the reaction was almost completed, the mixture was cooled to 0 °C and filtered under vacuum to give a yellow powder, which was washed with cold diethyl ether (3×20 mL). Finally, the desired compound **9** was obtained as a mixture with a small amount of the starting material **8** (0.22 g). The two compounds have the same R_f value based on TLC, which was confirmed by the ^{1}H NMR spectrum (Figure S32 in the Supporting Information).

Synthesis of azobenzene derivative G2: A solution of compound **9** (220 mg, also having a small amount of compound **8**) in ethanol (5.0 mL) and Me_3N (30% in water, 2.0 mL) was stirred at reflux temperature for 24 h. The solution was concentrated under reduced pressure. The residue was diluted with diethyl ether/CH_2Cl_2 (v/v = 5:1, 20.0 mL), the orange precipitate was collected by filtration and washed with diethyl ether/CH_2Cl_2 (v/v = 5:1) to remove compound **8**, and then the desired product **G2** was obtained as an orange solid (150 mg, about 95%). ^{1}H NMR (300 MHz, CD_3OD): δ = 8.03–7.93 (m, 4H), 7.86–7.65 (m, 4H), 4.64 (s, 2H), 3.13 (s, 9H), 2.41 (d, J = 6.6 Hz, 2H), 1.72 (s, 2H), 1.33 (br s, 16H), 0.89 ppm (br s, 3H); ^{13}C NMR (75 MHz, CD_3OD): δ = 173.6, 153.9, 148.5, 142.3, 133.7, 129.8, 123.7, 122.8, 119.6, 68.5, 51.9, 36.7, 31.7, 29.3, 29.2, 29.1, 28.9, 25.4, 22.3, 13.0 ppm; ESI-MS: m/z (%): 451.35 [M−Br]$^+$; HR-ESI-MS: m/z calcd for [M−Br]$^+$ $C_{28}H_{43}N_4O$: 451.3431; found: 451.3435.

Fabrication of the MTZ-loaded vesicles

MTZ-loaded vesicles were prepared as follows. A certain amount of MTZ was added to an aqueous solution of **G2** (1% EtOH was added to improve the solubility of **G2**), then a certain concentration of **WP6** solution was added quickly, and finally some water was added until the volume of the solution reached 25 mL. The ultimate concentrations of MTZ, **G2**, and **WP6** were 0.018, 0.09, and 0.01 mM, respectively. After standing overnight, the prepared MTZ-loaded vesicles were purified by dialysis (molecular weight cutoff 10000) in distilled water several times until the water outside the dialysis tube exhibited negligible MTZ fluorescence. For the cell experiments, MTZ-loaded vesicles were prepared in PBS buffer by using the same procedure as mentioned above.

The MTZ encapsulation efficiency was calculated by the following equation [Eq. (1)],[7e] in which $m_{\text{MTZ-loaded}}$ and m_{MTZ} are the mass of MTZ encapsulated in vesicles and mass of MTZ added, respectively. The mass of MTZ was measured by a UV spectrophotometer at 660 nm and calculated relative to a standard calibration curve at concentrations from 0.184 to 6.68 $\mu g\,mL^{-1}$ in water.

$$\text{Encapsulation efficiency}\ (\%) = (m_{\text{MTZ-loaded}}/m_{\text{MTZ}}) \times 100 \qquad (1)$$

Stimuli-responsive behaviors of the MTZ-loaded vesicles

pH-Responsive drug release in vitro: Tris-HCl buffer solutions (0.01 M, pH 7.4), citrate buffer solutions (0.05 M, pH 6.2), and sodium acetate buffer solutions (0.05 M, pH 4.4) were used as drug release media to simulate normal physiological conditions and the intracellular conditions of tumors. In a typical release experiment, MTZ-loaded vesicles (15 mL) were added to an appropriate release medium (10 mL) at 37 °C. At selected time intervals, a portion (2 mL) of the release medium was taken out for measuring of the released MTZ concentration by the UV/Vis absorption technique. A nearly 100% release of MTZ from MTZ-loaded vesicles was obtained by using a very low pH medium (solution of HCl, pH 3) in which most of the vesicles collapsed.

UV-Responsive drug release in vitro: To investigate the UV-responsive behaviors of the **WP6⊃G2** supramolecular vesicles, the MTZ-loaded vesicular solution was placed vertically under a high-pressure mercury lamp (365 nm, 200 W) at a distance of 10 cm. In the cell experiments, an ultraviolet lamp (365 nm, 25 W) was used.

Dual pH- and UV-responsive drug release in vitro: For the dual pH- and UV-responsive release experiments of MTZ-loaded vesicles, the detailed procedures were almost the same as those for the pH-responsive experiments mentioned above, but additionally, the vesicular solution was placed vertically under a high-pressure mercury lamp (365 nm, 200 W) at a distance of 10 cm, and detected at selected time intervals. The concentration of MTZ was determined by measuring the absorbance at 660 nm by using a standard absorbance versus concentration curve constructed for MTZ in the corresponding release buffer.

Cytotoxicity measurement

Cell culture: MCF-7 cancer cells (a human breast cancer cell line) and NIH3T3 normal cells (a mouse embryonic fibroblast cell line) were cultivated, respectively, in Dulbecco's modified Eagle's medium (DMEM) supplied with 10% fetal bovine serum (FBS) and antibiotics (50 $U\,mL^{-1}$ penicillin and 50 $U\,mL^{-1}$ streptomycin) at 37 °C in a humidified atmosphere containing 5% CO_2.

MTT assay: The relative cytotoxicities of **G2**, unloaded vesicles, MTZ, and MTZ-loaded vesicles against NIH3T3 normal cells and MCF-7 cancer cells were evaluated in vitro by 3-(4,5-dimethylthiazol-2-yl)-2,5-diphenyltetrazolium bromide (MTT) assay. Briefly, the cells were seeded in 96-well plates at a density of 1.0×10^5 cells per well in complete DMEM (200 μL) containing 10% FBS supplemented with penicillin (50 $U\,mL^{-1}$) and streptomycin (50 $U\,mL^{-1}$), and cultured in 5% CO_2 at 37 °C for 24 h. Then NIH3T3 cells were incubated with **G2**, unloaded vesicles, MTZ, and MTZ-loaded vesicles. MCF-7 cells were subsequently incubated with unloaded vesicles, MTZ, and MTZ-loaded vesicles. The ultimate concentrations of MTZ, **WP6**, and **G2** were 0.94, 0.7, and 6.3 μM, respectively. For UV-stimulus experiments, the cells were irradiated under UV light at 365 nm (25 W) for 30 min after incubation with MTZ-loaded vesicles for 3 h and cultured for another 24 h, and then the UV irradiation procedure was repeated. At the end of each incubation (24, 48, 72, or 96 h), the cells were washed, replenished with fresh culture medium, and further incubated for 2 h. Subsequently, MTT solution (20 μL) was added to each well and incubated for another 4 h. After that, the medium containing MTT was removed and dimethyl sulfoxide (DMSO, 100 μL) was added to each well to dissolve the MTT formazan crystals. Finally, the plates were shaken for 10 min, and the absorbance of formazan product was measured at 490 nm by a microplate reader (BioTek ELx808). Untreated cells in media were used as the blank control. All experiments were carried out with three replicates. The cytotoxicity was expressed as the percentage of the cell viability relative to the blank control.

Apoptosis assay: MCF-7 cells were seeded in 12-well plates at a density of 1.0×10^5 cells per well in DMEM culture medium (1 mL), cultured for 24 h, and then the culture medium was removed. MTZ-loaded vesicles dissolved in DMEM culture medium at a final concentration of 0.94 μM were added to the wells (1 $mL\,well^{-1}$) and the cells were incubated at 37 °C for 48 and 96 h. MCF-7 cells without incubation of MTZ-loaded vesicles were used as control. After incubation for 48 and 96 h, the cell solutions were centrifuged for 5 min at 2000 rpm. Culture medium was removed and the cells were washed with cold PBS twice. After removal of the supernatants, the cells were resuspended in binding buffer (500 μL). The apoptotic cells were determined by staining using an Annexin V-FITC apoptosis detection kit according to the manufacturer's protocol: Annexin V-FITC (5 μL) and PI (5 μL, provided in the kit) were added to the cell suspensions; after incubation in the dark for 15 min, data for 1.0×10^4 gated events were collected and analyzed by a BD FACSCalibur flow cytometer and CELLQuest software.

Statistical analysis

Differences between treatment groups were analyzed statistically using Student's *t*-test. A statistically significant difference was reported if $p<0.05$. The data were expressed as the mean ± standard deviation from at least three separate experiments.

Acknowledgements

This work was supported by the National Basic Research Program of China (2014CB846000, 2013CB934400), and National Natural Science Foundation of China (Nos. 91227106, 21202083, 21302092). We wish to thank Professor Dongzhong Chen from Nanjing University for fruitful discussions and suggestions.

Keywords: drug delivery · micelles · pillararenes · supramolecular chemistry · vesicles

[1] B. W. Stewart, P. Kleihues, *World Cancer Report*, World Health Organization Press, Geneva, **2003**.

[2] a) J. W. Singer, R. Bhatt, J. Tulinsky, K. R. Buhler, E. Heasley, P. Klein, P. de Vries, *J. Controlled Release* **2001**, *74*, 243 – 247; b) P. A. McCarron, W. M. Marouf, D. J. Quinn, F. Fay, R. E. Burden, S. A. Olwill, C. J. Scott, *Bioconjugate Chem.* **2008**, *19*, 1561 – 1569; c) C. Shi, X. Guo, Q. Qu, Z. Tang, Y. Wang, S. Zhou, *Biomaterials* **2014**, *35*, 8711 – 8722; d) I. Fischer, K. Petkau-Milroy, Y. L. Dorland, A. P. H. J. Schenning, L. Brunsveld, *Chem. Eur. J.* **2013**, *19*, 16646 – 16650.

[3] a) R. K. Jain, *J. Controlled Release* **2001**, *74*, 7 – 25; b) C. Barbé, J. Bartlett, L. Kong, K. Finnie, H. Q. Lin, M. Larkin, S. Calleja, A. Bush, G. Calleja, *Adv. Mater.* **2004**, *16*, 1959 – 1966.

[4] B. J. Ravoo in *Supramolecular Chemistry: from Molecules to Nanomaterials, Vol. 2* (Ed.: J. W. Steed, Gale, P. A.), Wiley, Chichester, **2012**, pp. 501 – 514.

[5] a) X. Zhang, C. Wang, *Chem. Soc. Rev.* **2011**, *40*, 94 – 101; b) C. Wang, Z. Wang, X. Zhang, *Acc. Chem. Res.* **2012**, *45*, 608 – 618.

[6] a) Q. Duan, Y. Cao, Y. Li, X. Hu, T. Xiao, C. Lin, Y. Pan, L. Wang, *J. Am. Chem. Soc.* **2013**, *135*, 10542 – 10549; b) Y. Cao, X.-Y. Hu, Y. Li, X. Zou, S. Xiong, C. Lin, Y.-Z. Shen, L. Wang, *J. Am. Chem. Soc.* **2014**, *136*, 10762 – 10769; c) G. Yu, X. Zhou, Z. Zhang, C. Han, Z. Mao, C. Gao, F. Huang, *J. Am. Chem. Soc.* **2012**, *134*, 19489 – 19497.

[7] K. Wang, D.-S. Guo, Y. Liu, *Chem. Eur. J.* **2010**, *16*, 8006 – 8011.

[8] a) R. L. McCarley, *Annu. Rev. Anal. Chem.* **2012**, *5*, 391 – 411; b) C. Wang, Y. Guo, Y. Wang, H. Xu, X. Zhang, *Chem. Commun.* **2009**, 5380 – 5382.

[9] Q. Yan, J. Yuan, Z. Cai, Y. Xin, Y. Kang, Y. Yin, *J. Am. Chem. Soc.* **2010**, *132*, 9268 – 9270.

[10] D.-S. Guo, K. Wang, Y.-X. Wang, Y. Liu, *J. Am. Chem. Soc.* **2012**, *134*, 10244 – 10250.

[11] a) Y. Wang, N. Ma, Z. Wang, X. Zhang, *Angew. Chem. Int. Ed.* **2007**, *46*, 2823 – 2826; *Angew. Chem.* **2007**, *119*, 2881 – 2884; b) D. Xia, G. Yu, J. Li, F. Huang, *Chem. Commun.* **2014**, *50*, 3606 – 3608.

[12] a) Y. H. Ko, E. Kim, I. Hwang, K. Kim, *Chem. Commun.* **2007**, 1305 – 1315; b) C. Wang, S. Yin, S. Chen, H. Xu, Z. Wang, X. Zhang, *Angew. Chem. Int. Ed.* **2008**, *47*, 9049 – 9052; *Angew. Chem.* **2008**, *120*, 9189 – 9192; c) Y. J. Jeon, P. K. Bharadwaj, S. Choi, J. W. Lee, K. Kim, *Angew. Chem. Int. Ed.* **2002**, *41*, 4474 – 4476; *Angew. Chem.* **2002**, *114*, 4654 – 4656; d) J. Zou, F. Tao, M. Jiang, *Langmuir* **2007**, *23*, 12791 – 12794; e) D. Jiao, J. Geng, X. J. Loh, D. Das, T.-C. Lee, O. A. Scherman, *Angew. Chem. Int. Ed.* **2012**, *51*, 9633 – 9637; *Angew. Chem.* **2012**, *124*, 9771 – 9775; f) G. Yu, M. Xue, Z. Zhang, J. Li, C. Han, F. Huang, *J. Am. Chem. Soc.* **2012**, *134*, 13248 – 13251.

[13] K. Wang, D.-S. Guo, X. Wang, Y. Liu, *ACS Nano* **2011**, *5*, 2880 – 2894.

[14] a) Y.-C. Wang, Y. Li, X.-Z. Yang, Y.-Y. Yuan, L.-F. Yan, J. Wang, *Macromolecules* **2009**, *42*, 3026 – 3032; b) J. Liu, Y. Pang, W. Huang, X. Zhu, Y. Zhou, D. Yan, *Biomaterials* **2010**, *31*, 1334 – 1341; c) J. Liu, W. Huang, Y. Pang, X. Zhu, Y. Zhou, D. Yan, *Biomaterials* **2010**, *31*, 5643 – 5651.

[15] a) T. Ogoshi, S. Kanai, S. Fujinami, T.-a. Yamagishi, Y. Nakamoto, *J. Am. Chem. Soc.* **2008**, *130*, 5022 – 5023; b) M. Xue, Y. Yang, X. Chi, Z. Zhang, F. Huang, *Acc. Chem. Res.* **2012**, *45*, 1294 – 1308; c) T. Ogoshi, *J. Inclusion Phenom. Macrocyclic Chem.* **2012**, *72*, 247 – 262.

[16] a) Y. Yao, M. Xue, J. Chen, M. Zhang, F. Huang, *J. Am. Chem. Soc.* **2012**, *134*, 15712 – 15715; b) H. Zhang, X. Ma, K. T. Nguyen, Y. Zhao, *ACS Nano* **2013**, *7*, 7853 – 7863; c) Y.-L. Sun, Y.-W. Yang, D.-X. Chen, G. Wang, Y. Zhou, C.-Y. Wang, J. F. Stoddart, *Small* **2013**, *9*, 3224 – 3229.

[17] a) G. Yu, Z. Zhang, C. Han, M. Xue, Q. Zhou, F. Huang, *Chem. Commun.* **2012**, *48*, 2958 – 2960; b) S. Sun, X.-Y. Hu, D. Chen, J. Shi, Y. Dong, C. Lin, Y. Pan, L. Wang, *Polym. Chem.* **2013**, *4*, 2224 – 2229; c) S. Sun, J.-B. Shi, Y.-P. Dong, C. Lin, X.-Y. Hu, L.-Y. Wang, *Chin. Chem. Lett.* **2013**, *24*, 987 – 992; d) X. Shu, S. Chen, J. Li, Z. Chen, L. Weng, X. Jia, C. Li, *Chem. Commun.* **2012**, *48*, 2967 – 2969.

[18] a) W. Si, L. Chen, X.-B. Hu, G. Tang, Z. Chen, J.-L. Hou, Z.-T. Li, *Angew. Chem. Int. Ed.* **2011**, *50*, 12564 – 12568; *Angew. Chem.* **2011**, *123*, 12772 – 12776; b) L. Chen, W. Si, L. Zhang, G. Tang, Z.-T. Li, J.-L. Hou, *J. Am. Chem. Soc.* **2013**, *135*, 2152 – 2155; c) W. Si, Z.-T. Li, J.-L. Hou, *Angew. Chem. Int. Ed.* **2014**, *53*, 4578 – 4581; *Angew. Chem.* **2014**, *126*, 4666 – 4669.

[19] a) Z. Zhang, Y. Luo, J. Chen, S. Dong, Y. Yu, Z. Ma, F. Huang, *Angew. Chem. Int. Ed.* **2011**, *50*, 1397 – 1401; *Angew. Chem.* **2011**, *123*, 1433 – 1437; b) X.-Y. Hu, X. Wu, Q. Duan, T. Xiao, C. Lin, L. Wang, *Org. Lett.* **2012**, *14*, 4826 – 4829; c) Y. Guan, M. Ni, X. Hu, T. Xiao, S. Xiong, C. Lin, L. Wang, *Chem. Commun.* **2012**, *48*, 8529 – 8531; d) X.-Y. Hu, X. Wu, S. Wang, D. Chen, W. Xia, C. Lin, Y. Pan, L. Wang, *Polym. Chem.* **2013**, *4*, 4292 – 4297; e) C. Li, *Chem. Commun.* **2014**, *50*, 12420 – 12433.

[20] a) A. Altieri, G. Bottari, F. Dehez, D. A. Leigh, J. K. Y. Wong, F. Zerbetto, *Angew. Chem. Int. Ed.* **2003**, *42*, 2296 – 2300; *Angew. Chem.* **2003**, *115*, 2398 – 2402; b) X. Liu, M. Jiang, *Angew. Chem. Int. Ed.* **2006**, *45*, 3846 – 3850; *Angew. Chem.* **2006**, *118*, 3930 – 3934.

[21] G. Yu, C. Han, Z. Zhang, J. Chen, X. Yan, B. Zheng, S. Liu, F. Huang, *J. Am. Chem. Soc.* **2012**, *134*, 8711 – 8717.

[22] G. R. Wiese, T. W. Healy, *Trans. Faraday Soc.* **1970**, *66*, 490 – 499.

[23] a) G. Wang, X. Tong, Y. Zhao, *Macromolecules* **2004**, *37*, 8911 – 8917; b) H. Yu, T. Iyoda, T. Ikeda, *J. Am. Chem. Soc.* **2006**, *128*, 11010 – 11011; c) Z. Shi, D. Chen, H. Lu, B. Wu, J. Ma, R. Cheng, J. Fang, X. Chen, *Soft Matter* **2012**, *8*, 6174 – 6184.

[24] K. Ariga, Q. Ji, J. P. Hill, N. Kawazoe, G. Chen, *Exp. Opin. Biol. Ther.* **2009**, *9*, 307 – 320.

[25] a) C. Dugave, L. Demange, *Chem. Rev.* **2003**, *103*, 2475 – 2532; b) L. L. Zhu, M. Q. Lu, Q. W. Zhang, D. H. Qu, H. Tian, *Macromolecules* **2011**, *44*, 4092 – 4097; c) L. Zhu, H. Yan, X.-J. Wang, Y. Zhao, *J. Org. Chem.* **2012**, *77*, 10168 – 10175.

[26] a) B. S. Parker, T. Buley, B. J. Evison, S. M. Cutts, G. M. Neumann, M. N. Iskander, D. R. Phillips, *J. Biol. Chem.* **2004**, *279*, 18814 – 18823; b) J. Mazerski, S. Martelli, E. Borowski, *Acta Biochim. Pol.* **1998**, *45*, 1 – 11.

[27] a) J. Panyam, V. Labhasetwar, *Adv. Drug Delivery Rev.* **2003**, *55*, 329 – 347; b) M. Nagae, T. Hiraga, T. Yoneda, *J. Bone Miner. Metab.* **2007**, *25*, 99 – 104.

[28] a) M. Stubbs, P. M. J. McSheehy, J. R. Griffiths, C. L. Bashford, *Mol. Med. Today* **2000**, *6*, 15 – 19; b) G. Liu, X. Li, S. Xiong, L. Li, P. Chu, K. K. Yeung, S. Wu, Z. Xu, *Colloid Polym. Sci.* **2012**, *290*, 349 – 357.

[29] B.-C. Yu, Y. Shirai, J. M. Tour, *Tetrahedron* **2006**, *62*, 10303 – 10310.

Received: September 2, 2014
Published online on ■■ ■■, 0000

FULL PAPER

Drug Delivery

*X.-Y. Hu, K. Jia, Y. Cao, Y. Li, S. Qin, F. Zhou, C. Lin, D. Zhang, L. Wang**

■■ – ■■

Dual Photo- and pH-Responsive Supramolecular Nanocarriers Based on Water-Soluble Pillar[6]arene and Different Azobenzene Derivatives for Intracellular Anticancer Drug Delivery

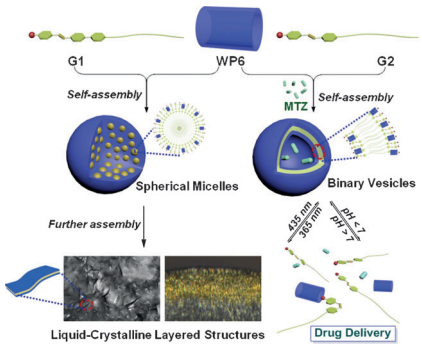

On the double: Two types of nanocarriers are fabricated: supramolecular micelles formed from water-soluble pillar[6]arene (**WP6**) and azobenzene derivative **G1**, which gradually transform into layered structures, and supramolecular vesicles formed by **WP6** and guest **G2**, which exhibit dual photo- and pH-responsive behavior (see figure). Mitoxantrone (MTZ)-loaded vesicles show a similar therapeutic effect for cancer cells to free MTZ and reduced damage to normal cells.